Orientationally invariant axon-size and density weighted MRI

D. C. Alexander[1], P. L. Hubbard[2], M. G. Hall[1], E. A. Moore[3], M. Ptito[4], G. J. Parker[2], and T. B. Dyrby[5]

[1]Centre for Medical Image Computing, Dept. Computer Science, UCL (University College London), London, United Kingdom, [2]Imaging Science and Biomedical Engineering, School of Cancer and Imaging Sciences, University of Manchester, Manchester, United Kingdom, [3]Best, Philips Healthcare, Eindhoven, Netherlands, [4]School of Optometry, University of Montreal, Montreal, Canada, [5]Danish Research Centre for Magnetic Resonance, Copenhagen University Hospital, Copenhagen, Denmark

Introduction: We present a new model-based diffusion MRI technique for mapping correlates of the axon size and density in white matter. The parameters offer new insight in the brain and more natural biomarkers than standard indices like FA. Similar model-based approaches [1,2] show good agreement with histological measurements on fixed samples and a live rat [3], but have three key limitations: they require high gradient strengths (300mT/m in [3]), long acquisition times (2h in [3]) and knowledge of the fibre orientation. The last limitation is most fundamental and prevents whole brain parameter mapping. The active imaging approach in [4] optimizes an orientationally invariant protocol and simulations suggest feasibility of estimating axon size and density with achievable acquisition and unspecified fibre orientation. Here, we use the approach to map axon-size and density indices over a perfusion fixated velveteen monkey brain, prepared as in [5], and a live human brain.

Method: The optimization in [4] provides protocols for the monkey brain on a 4.7T Varian experimental system with maximum gradient strength $|\mathbf{G}|_{max}$=140mT/m and for the live human brain on a clinical 3T Philips Achieva system with $|\mathbf{G}|_{max}$=60mT/m. Both protocols contain four PGSE sequences to acquire in each of 90 evenly distributed gradient directions. The monkey protocol has three unique measurements with b values 1668, 3354 and 14046 smm^{-2} (the second is duplicated); the human protocol has b values of 529, 704, 2721, 2784 smm^{-2} (the last two are almost identical). The monkey data set has two repeats of each measurement, 24 b=0 images and took 150h. The human data set includes 4 b=0 images and took less than 1h. White matter SNR at b=0 is about 20 in both.

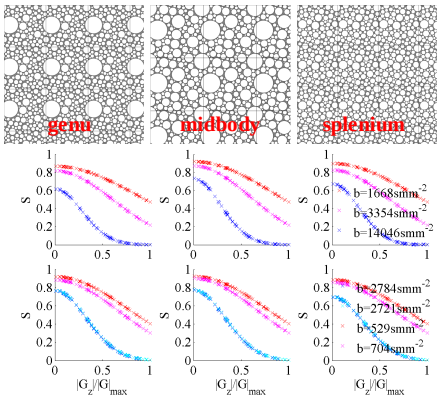

Fig. 1: Example synthetic substrates (top), synthetic signals from monkey protocol (middle) and from human protocol (bottom).

We fit a model that simplifies the AxCaliber model in [3], which includes an isotropic compartment to account for partial volume. We assume a single axon radius, as in [4], and a tortuosity model, as in [1]. The final axon-size statistic R is the mean of the posterior distribution on the model's radius parameter, which we sample using MCMC, as in [4]. The axon density statistic is $a=f/\pi R^2$, where f is the intracellular volume fraction of the anisotropic compartment.

Results: Simulation experiments generate synthetic geometric models, as in [6], for different parts of the corpus callosum (CC). The models are parallel cylinders along the z-axis with radius distributions matching data in [7,8]. Figure 1 shows three simulated examples for sections of the CC using [7] and plots the normalized signal S from Monte-Carlo diffusion simulations [6] within each for both the monkey and human protocols with free diffusivities of 0.45μm^2/ms and 1.7μm^2/ms, respectively. Qualitative differences (compare the perpendicular signals where $|\mathbf{G}|_z$=0) suggest the optimized protocols distinguish the microstructures.

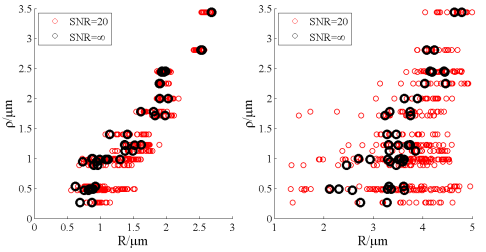

Fig. 2: R v ρ simulation. Monkey left; human right.

We hypothesize that R correlates with $\rho=\int r^2 p(r)dr$, where p is the true distribution of radii r, since the contribution of each cylinder is proportional to its volume. Figure 2 plots R from noisy and noise-free synthetic data against ρ for a variety of radius distributions and densities from [7,8]. In the absence of noise, R correlates well with ρ for the monkey protocol, but underestimates at high ρ and overestimates at low ρ. For the human protocol, R also correlates, but less strongly, and consistently overestimates ρ. The estimates from noisy data still correlate with ρ.

Figure 3 maps R and a over regions of high diffusion-tensor linearity and low planarity in the mid-sagittal slice of the monkey. Histological data from the CC in [7,8] show that ρ goes from low to high to low from genu to mid-body to splenium, whereas the density goes from high to low to high. The maps of R and a show these patterns in the CC, although, as in the simulations, R tends to overestimate ρ, which artificially reduces a. Low R is less consistent in the genu than the splenium. The mean R/μm and a/μm^{-2} in the genu, midbody and splenium are (2.3, 0.2), (2.6, 0.1), (1.5, 1.2). Figure 4 shows similar maps for the human over a sagittal slice 12mm from the midline. Orientational invariance is essential in this slice where the CC orientation varies front to back. The slice also contains part of the cortico-spinal tract, which has low density, high ρ and runs up-down. In the CC, the high-low-high trend in a is visible, but low-high-low in R is less obvious. However, mean R/μm and a/μm^{-2} in the genu, midbody and splenium are (2.9, 0.05), (4.0, 0.02), (2.9, 0.05). The values are similar at the midline. Mean values are (4.6, 0.01) in the CST.

Discussion: The method estimates new parameters that correlate with axon size and density and do not require known fibre orientation. Spatial variation matches known histology most clearly in the monkey brain, but is also detectable in the human. Higher $|\mathbf{G}|_{max}$ and SNR will improve precision. We consistently see the trends in different human subjects, although absolute values vary. Future work will address the instability.

1 Stanisz MRM95. 2 Assaf MRM08. 3 Barazany ISMRM08. 4 Alexander MRM08. 5 Dyrby ISMRM08. 6 Hall CDMRI08. 7 Aboitiz B. Res. 92. 8 Lamantia JCN90.

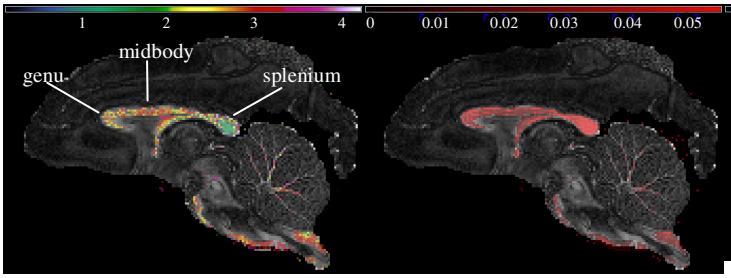

Fig. 3: Maps of R/μm (left) and a/μm^{-2} (right) from monkey overlaid on FA.

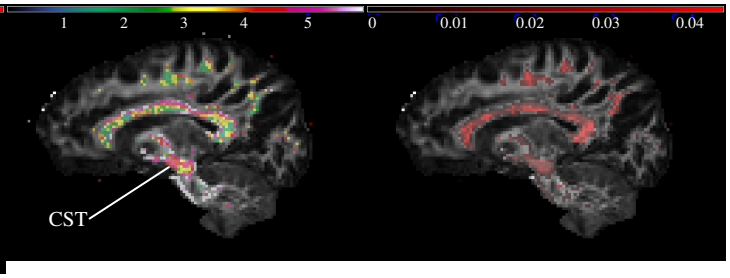

Fig. 4: Maps of R/μm (left) and a/μm^{-2} (right) for human overlaid on FA.